Biochemical Journal (2020) **477** 4149–4165
https://doi.org/10.1042/BCJ20200592

Research Article

Functional analysis of a species-specific inhibitor selective for human Na^+-coupled citrate transporter (NaCT/SLC13A5/mINDY)

Kei Higuchi[1], Jonathan J. Kopel[1], Sathish Sivaprakasam[1], Valeria Jaramillo-Martinez[2], R. Bryan Sutton[3,4], Ina L. Urbatsch[1,4] and Vadivel Ganapathy[1,4]

[1]Department of Cell Biology and Biochemistry, Texas Tech University Health Sciences Center, Lubbock 79430, Texas, U.S.A.; [2]Department of Pharmacology and Neuroscience, Texas Tech University Health Sciences Center, Lubbock 79430, Texas, U.S.A.; [3]Department of Cell Physiology and Molecular Biophysics, Texas Tech University Health Sciences Center, Lubbock 79430, Texas, U.S.A.; [4]Center for Membrane Protein Research, Texas Tech University Health Sciences Center, Lubbock 79430, Texas, U.S.A.

Correspondence: Vadivel Ganapathy (vadivel.ganapathy@ttuhsc.edu)

The Na^+-coupled citrate transporter (NaCT/SLC13A5/mINDY) in the liver delivers citrate from the blood into hepatocytes. As citrate is a key metabolite and regulator of multiple biochemical pathways, deletion of Slc13a5 in mice protects against diet-induced obesity, diabetes, and metabolic syndrome. Silencing the transporter suppresses hepatocellular carcinoma. Therefore, selective blockers of NaCT hold the potential to treat various diseases. Here we report on the characteristics of one such inhibitor, BI01383298. It is known that BI01383298 is a high-affinity inhibitor selective for human NaCT with no effect on mouse NaCT. Here we show that this compound is an irreversible and non-competitive inhibitor of human NaCT, thus describing the first irreversible inhibitor for this transporter. The mouse NaCT is not affected by this compound. The inhibition of human NaCT by BI01383298 is evident for the constitutively expressed transporter in HepG2 cells and for the ectopically expressed human NaCT in HEK293 cells. The IC_{50} is ~100 nM, representing the highest potency among the NaCT inhibitors known to date. Exposure of HepG2 cells to this inhibitor results in decreased cell proliferation. We performed molecular modeling of the 3D-structures of human and mouse NaCTs using the crystal structure of a humanized variant of VcINDY as the template, and docking studies to identify the amino acid residues involved in the binding of citrate and BI01383298. These studies provide insight into the probable bases for the differential effects of the inhibitor on human NaCT versus mouse NaCT as well as for the marked species-specific difference in citrate affinity.

Introduction

Obesity and obesity-related comorbidities have become a big burden on healthcare cost. Obese patients develop metabolic syndrome, a constellation of biochemical/clinical abnormalities including insulin resistance, hypertension, and dyslipidemia (decreased HDL, increased LDL, hypercholesterolemia, and hypertriglyceridemia) [1,2]. The organs/tissues damaged in metabolic syndrome include heart, blood vessels, pancreas, kidney, and liver. If left untreated, metabolic syndrome increases the morbidity and mortality arising from the compromised functions of these organs/tissues. Current guidelines for the treatment of metabolic syndrome emphasize lifestyle interventions such as weight reduction, exercise, and decreased caloric intake [3]. However, patients often have difficulty in adhering to these guidelines. Without success in these lifestyle interventions, medications are being sought to effectively manage metabolic syndrome.

Received: 30 July 2020
Revised: 12 October 2020
Accepted: 20 October 2020

Accepted Manuscript online: 20 October 2020
Version of Record published: 5 November 2020

PORTLAND PRESS

Biochemical Journal (2020) **477** 4149–4165
https://doi.org/10.1042/BCJ20200592

The plasma membrane citrate transporter NaCT/SLC13A5, also known as mINDY or mammalian orthologue of *Drosophila* INDY (I'm Not Dead Yet), has been recognized in recent years as an attractive target for treating obesity and metabolic syndrome [4,5]. Cytoplasmic citrate sits at the junction of many key metabolic pathways [6,7], including the synthesis of fatty acids and cholesterol. Citrate in the cytoplasm is also involved in the generation of NADPH via isocitrate dehydrogenases 1 and 2 following the conversion of citrate into isocitrate, and NADPH supplies reducing equivalents for the synthesis of fatty acids and cholesterol, and to support the cellular antioxidant machinery. Cytoplasmic citrate also inhibits fatty acid oxidation in mitochondria indirectly by serving as the source of acetyl CoA, a potent activator of acetyl CoA carboxylase, to generate malonyl CoA, which is an intermediate in fatty acid synthesis and also an inhibitor of carnitine-palmitoyl transferase-1, thus preventing the entry of long-chain fatty acids into mitochondria for subsequent oxidation. In addition, cytoplasmic citrate suppresses glycolysis by inhibiting phosphofructokinase-1 and stimulates gluconeogenesis by activating fructose-1,6-bisphosphatase. Citrate in the cytoplasm was thought to arise solely from mitochondria via the citrate carrier (SLC25A1) located in the inner mitochondrial membrane. However, the discovery of the plasma membrane citrate transporter (NaCT/SLC13A5/mINDY) laid the foundation for a paradigm shift in the field and highlights a second source for the cytoplasmic citrate, namely transfer of circulating citrate across the plasma membrane [8–11]. This is important considering the fact that citrate is present at significant concentrations (~200 μM) in blood [7]. The liver has robust activity for all of the metabolic pathways impacted by citrate. NaCT is expressed at the highest level in the liver [9,12] and is located on the sinusoidal membrane that is in contact with blood, an ideal location to facilitate the entry of citrate from the circulation into hepatocytes. Thus, NaCT plays a key role in this organ in promoting the synthesis of fatty acids and cholesterol, inhibiting fatty acid oxidation, decreasing glucose disposal via glycolysis and increasing gluconeogenesis; these represent major metabolic pathways associated with obesity, diabetes, and metabolic syndrome. Pharmacologic blockade of this transporter would therefore have beneficial impact in patients with these diseases. In support of this notion, NaCT/Slc13a5-knockout mice are leaner and resistant to diet-induced obesity and metabolic syndrome [4,13].

Over the past decade, several attempts have been made to develop potent and effective inhibitors for NaCT [14–18]. The first small-molecule inhibitors of NaCT were identified by screening ZINC database using the Docking module of Molecular Operating Environment [14]; this screening used the 3D model of NaCT deduced by homology modeling with LeuT, a bacterial amino acid transporter whose crystal structure was known by that time [19]. This search yielded two compounds (39396 and 4180643 in the ZINC database), both of which inhibit human NaCT noncompetitively with K_i values of 0.34 mM and 0.30 mM, respectively. Then came the discovery of the Pfizer compounds which were identified by virtual search of a Pfizer's compound library for structural similarities with citrate, the NaCT substrate [15,18]. Transport assays with human NaCT showed that the compound PF-06649298 was the most potent inhibitor of NaCT-mediated citrate uptake with an IC_{50} value of 0.4–10 μM [15]. This compound is a transportable substrate for NaCT and competes with citrate for the transport process; it has no species selectivity however, with ability to inhibit mouse and human NaCTs [15]. The binding of this molecule to human NaCT was assessed theoretically using the Docking module with the 3D structure of the transporter based on the homology modeling with a bacterial dicarboxylate transporter known as VcINDY [16]. VcINDY serves as a more appropriate template than LeuT to model NaCT based on the class of substrates for these two transporters: carboxylates for VcINDY and amino acids for LeuT. The structure of PF-06649298 was further optimized to increase the inhibitor potency by ~4-fold [17]. Even though PF-06649298 and its derivative PF-06761281 competed with citrate for the substrate-binding site, the inhibitory potency was surprisingly higher with increasing citrate concentrations. These data suggested that these compounds are actually allosteric inhibitors whose interaction with NaCT is dependent on the state of the transporter with regard to citrate binding [18]. Recently, a new molecule, identified as BI01383298, has been shown as a highly potent inhibitor of human NaCT with an IC_{50} of 25–60 nM, significantly more potent than PF-06649298 (IC_{50}, 0.4–10 μM). Interestingly, this new compound inhibits only human NaCT and has no effect on mouse NaCT. This information on the affinity and species-specificity of BI01383298 is available only from the Structural Genomics Consortium, a public-private partnership that supports the discovery of new medicines through open-access research. There is no published report on this inhibitor. Here we investigated the functional features of BI01383298 as an inhibitor of NaCT and deduced the molecular basis of its species specificity based on structural modeling and molecular docking strategies.

Biochemical Journal (2020) 477 4149–4165
https://doi.org/10.1042/BCJ20200592

Materials and methods

Materials

BI01383298, 1-(3,5-Dichlorophenylsulfonyl)-N-(4-fluorobenzyl)piperidine-4-carboxamide, was purchased from Medkoo Biosciences (Chapel Hill, NC, U.S.A.). BI01372674, chemically analogous to BI01383298, was provided by Boehringer Ingelheim Pharma GmbH (Ingelheim, Germany). PF06761281, (2R)-2-Hydroxy-2-[2-(2-methoxy-5-methyl-3-pyridinyl)ethyl]succinic acid, was kindly supplied by Pfizer Inc. (New York, NY, U.S.A.). [^{14}C]-Citrate (specific radioactivity, 113 mCi/mmol) and [^{14}C]-nicotinate (specific radioactivity, 50 mCi/mmol) were purchased from Moravek Biochemicals (Brea, CA, U.S.A.). [^{3}H]-Arginine monohydrochloride (specific radioactivity, 54.5 mCi/mmol), [^{14}C]-lactate (specific radioactivity, 154.8 mCi/mmol), [^{3}H]-glutamine (specific radioactivity, 50.5 mCi/mmol), and [^{3}H]-tryptophan (specific radioactivity, 20.1 mCi/mmol) were purchased from PerkinElmer (Waltham, MA, U.S.A.). All other reagents were from Millipore-Sigma (St. Louis, MO, U.S.A.) or Thermo Fisher Scientific (Waltham, MA, U.S.A.).

Cell lines and culture conditions

Human hepatocellular carcinoma cell line HepG2 (RRID: CVCL_0027) and HEK293FT (RRID: CVCL_6911) were purchased from the American Type Culture Collection (ATCC, Manassas, VA, U.S.A.) and Thermo Fisher Scientific (Waltham, MA, U.S.A.), respectively. HepG2 cells were cultured in high-glucose DMEM, supplemented with 10% fetal bovine serum (FBS), 1% penicillin/streptomycin, 1 mM pyruvate, and 1 mM non-essential amino acids. HEK293FT cells were cultured in high-glucose DMEM medium supplemented with 10% FBS and 1% penicillin/streptomycin. These cell lines were used between passages 3 and 13 in the experiments.

Ectopic expression of human SLC13A5 and mouse Slc13a5 in HEK293FT cells

HEK293FT cells were used for transient ectopic expression of the cloned human SLC13A5 [9] and mouse Slc13a5 [10] with lipofectamine-3000-based transfection system. The plasmids containing the cDNAs for these transporters have been described previously [9,10]; the expression of the cDNA was under the control of the CMV promoter in these plasmids.

Uptake measurement

HepG2 cells were seeded at 4×10^5 cells per well on 24-well culture plates and cultured for 1–2 days. HEK293FT cells were seeded at 2×10^5 cells per well on 24-well culture plates, cultured for 1 day, and then transfected with human SLC13A5/pcDNA3.1(+) or mouse SLC13A5/pcDNA3.1(+) using Lipofectamine-3000 (Thermo Fisher Scientific), according to the manufacturer's recommendations. Uptake measurements were made in HepG2 cells 48 h after the initial seeding to monitor the activity of the constitutively expressed SLC13A5. In the case of HEK293FT cells, uptake measurements were made 48 h after the transfection to monitor the ectopically expressed human SLC13A5 or mouse Slc13a5. To initiate the uptake of citrate, the culture medium was removed by aspiration and then the cells were incubated in a NaCl buffer (140 mM NaCl, 5.4 mM KCl, 1.8 mM $CaCl_2$, 0.8 mM $MgSO_4$, and 5 mM glucose, buffered with 25 mM Hepes/Tris, pH 7.5) with or without the NaCT inhibitor BI01383298 for the indicated time intervals. In some experiments with ectopically expressed human SLC13A5 in HEK293FT cells, the effects of the vehicle control (0.1% dimethylsulfoxide) or the inactive chemical analogue BI01372674 (10 μM in 0.1% dimethylsulfoxide) on the transporter activity were investigated. In the case of recovery experiments, the buffer with the inhibitor was removed from the wells, and the cells were washed at least twice with the NaCl buffer, and then incubated in the NaCl buffer or culture medium for the indicated time intervals. The transport function of SLC13A5 in these cells was monitored by measuring the uptake of [^{14}C]-citrate (0.1 μCi; 4 μM citrate) using the NaCl-uptake buffer with or without 10 mM LiCl because Li^+ is an activator of human SLC13A5 [11,20]. The transport function of mouse Slc13a5 was monitored in the NaCl buffer but without LiCl because Li^+ is an inhibitor of murine NaCT [11,20]. The uptake measurements were recorded using a 30 min period at 37°C. At the end of the incubation, the medium was removed, the cells washed with ice-cold uptake buffer, and the cells lysed to measure the radioactivity. To determine specifically the Na^+-dependent citrate uptake, the uptake in NMDG (*N*-methyl-D-glucamine)-Cl buffer (i.e. Na^+-free) was subtracted from the uptake in the NaCl buffer with or without 10 mM LiCl. The uptake values were normalized with the protein content of the cells, measured by a Pierce™ BCA Protein Assay Kit (Thermo Fisher Scientific, Waltham, MA, U.S.A.).

Biochemical Journal (2020) 477 4149–4165
https://doi.org/10.1042/BCJ20200592

To estimate the kinetic parameters, the uptake velocity of citrate at each concentration (0.5–30 mM, 30 min incubation) was calculated by subtraction of non-saturable component from the total uptake velocity. The non-saturable component was estimated by subjecting the uptake data to a transport model consisting of a single saturable transport system with Michaelis–Menten saturable kinetic characteristics and a non-carrier-mediated, non-saturable, diffusional component. The uptake velocity for the saturable component was plotted and analyzed using the Michaelis–Menten equation by GraphPad Prism 7.01 software (GraphPad, San Diego, CA, U.S.A.). The linear form of the Michaelis–Menten equation was also used to calculate the kinetic constants (Eadie–Hofstee plot).

Colony formation assay

Colony formation assay was done by seeding HepG2 cells at 5000 cells per well in six-well culture plates and culturing the cells in the normal medium with 0.1% dimethylsulfoxide or the medium with 5 or 10 μM BI01383298 (plus 0.1% dimethylsulfoxide). The medium was changed with fresh corresponding medium every other day for 10 days. At the end of the experiment, cells were washed with phosphate-buffered saline, fixed with methanol, and stained with KaryoMax Giemsa stain. The colonies were then photographed and then the stain was extracted and quantified.

Statistics

Uptake measurements were made in triplicate and the experiments were repeated twice with separate cultures. In all cases, data are expressed as means ± S. D., except for the values of IC_{50}, K_t and V_{max}. Statistical analyses and graphing were performed in GraphPad Prism 7.01 software. Statistical differences between control groups and experimental groups were analyzed by two-tailed unpaired Student's *t*-test, or by one-way analysis of variance (ANOVA) followed by Dunnett's or Tukey's test, for single and multiple comparisons; a $P < 0.05$ was considered significant. For these statistical tests, the normality was confirmed using the GraphPad Prism 7.01 software.

Homology modeling

The primary sequence alignments of human and mouse NaCT (accession numbers Q86YT5, Q67BT3, respectively) were performed using PROMALS3D [21]. Based on the resulting primary sequence alignment, homology models of human and mouse NaCT were computed using the MODELLER program [22]. The crystal structure of the humanized variant of the bacterial homologue sodium-dependent dicarboxylate transporter from *Vibrio cholerae* was used as the template structure (VcINDY, PDB: 5ULD) [23]. VcINDY shares ∼29% amino acid sequence identity with human and mouse NaCT, with a higher sequence conservation seen in the Na^+- and substrate-binding sites. The first molecule was built and copied, and then superimposed with the second molecule in VcINDY forming a homodimer. Some of the long loops predicted by MODELLER were modeled as α-helices based on secondary structure prediction (https://academic.oup.com/nar/article/42/W1/W337/2435518). The two Na^+ and the citrate ions were placed in both monomers according to the VcINDY co-ordinates.

Docking studies

To improve the models for molecular docking studies, the human and mouse NaCT homology models were embedded in a DOPC bilayer using Charmm-GUI (www.charmm-gui.org) [24]. The protein:membrane system was subjected to 100 ns of molecular dynamics simulation using NAMD [25]. After the simulation was completed, the prediction models were extracted from the final timesteps of the trajectory. These structures were docked with citrate, BI01383298 or PF06761281 using AutoDock/Vina used with USCF Chimera program [26,27]. The size of the grid was 20 × 20 × 20 (Å3). Na^+ and citrate were included to compare how the inhibitor interacted with the binding site. Our intension was to discover whether the citrate and Na^+ binding residues were consistent with the template structure that we used to generate the SLC13A5 model. The lowest energy homology model obtained directly from MODELLER positioned some of the rotamers for the substrate in random orientations. We used molecular docking and molecular dynamics simulation to orient the substrate-binding residues of SLC13A5 into a more chemically sensible position. As we were not interested in the dynamic properties of the rest of the model, we specifically focused on the snapshots of the equilibrated model for substrate binding to the transporter. We took the snapshot under these equilibrated conditions to identify the amino acid residues involved in the interaction with citrate and inhibitors.

Biochemical Journal (2020) **477** 4149–4165
https://doi.org/10.1042/BCJ20200592

Results

Time-dependent inhibition of NaCT by BI01383298 in HepG2 cells

First, we examined the effect of BI01383298 on NaCT-mediated citrate uptake in the human liver cell line HepG2, which constitutively expresses the transporter [20]. We did this experiment using the routine approach in which Na^+-coupled uptake of citrate (10 μM) was measured for 30 min with increasing concentrations of the inhibitor present only during the uptake assay. The uptake was inhibited by BI01383298 in a dose-dependent manner, but the maximal inhibition stopped at ∼60% (Figure 1A). We repeated the experiment in the presence of Li^+, which stimulates the transport function of human NaCT by increasing its affinity for citrate [20]. The inhibitory potency of BI01383298 increased significantly when monitored in the presence of Li^+, but still the maximal inhibition stopped at ∼60%. We thought that if the inhibitor needs time to interact with the transporter, that would at least partly explain the results. Therefore, we preincubated the cells with various concentrations of the inhibitor for 30 min and then measured Na^+-coupled citrate uptake with the inhibitor present also during uptake at the same concentrations as during preincubation. Under these conditions, BI01383298 was able to inhibit the transporter almost completely (Figure 1B). We repeated this experiment with Li^+ present during the uptake assay. Again, the inhibition was almost complete and the concentration needed for 50% inhibition was 2-fold lower in the presence of Li^+ than in its absence (49 ± 3 nM in the presence of Li^+; 118 ± 22 nM in the absence of Li^+). These values were significantly lower than the corresponding values when the cells were not preincubated with the inhibitor (∼0.5 μM in the presence of Li^+; 3 μM in the absence of Li^+) (Figure 1A). These data suggest that the inhibitory potency for BI01383298 increases by ∼10-fold, both in the absence or presence of Li^+, when the cells were subjected to preincubation with the inhibitor.

Irreversible nature of inhibition by BI01383298

As the interaction of BI01383298 with NaCT was found to become stronger with preincubation, we wanted to know whether the interaction was reversible or irreversible. To address this issue, we preincubated HepG2 cells with 10 μM of the inhibitor for varying periods of time and then washed the cells to remove any free inhibitor in the medium, and then used the cells to monitor NaCT activity (i.e. Na^+-coupled citrate uptake). The inhibitor was not present during the uptake assay. We found a decrease in NaCT uptake activity in a manner that

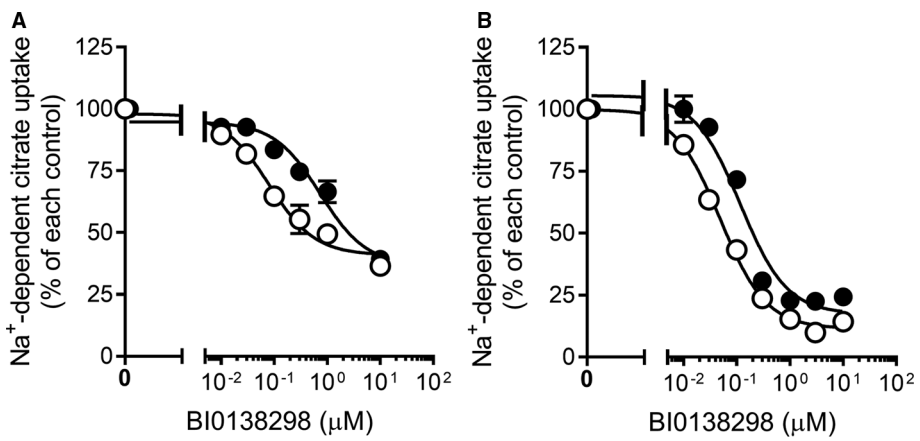

Figure 1. Inhibitory effect of BI01383298 on NaCT-mediated citrate uptake in HepG2 cells.
(**A**) HepG2 cells were co-incubated with BI01383298 and [^{14}C]-citrate. Uptake of [^{14}C]-citrate was measured for 30 min in NaCl buffer, pH 7.5, either without (●) or with 10 mM LiCl (○) with increasing concentrations of BI01383298. (**B**) HepG2 cells were first preincubated with increasing concentrations of BI0138298 in NaCl buffer, pH 7.5, either without (●) or with 10 mM LiCl buffer (○) for 30 min, and then uptake of [^{14}C]-citrate was measured for 30 min with the same respective preincubation buffer. In this case, the inhibitor was present at different concentrations both during preincubation as well as during uptake. The uptake values were markedly higher when measured in the presence of Li^+ than in the absence of Li^+ as expected of human NaCT. The concentration of citrate was 7.0 μM for the uptake assay in the absence of Li^+, and 3.5 μM for the uptake assay in the presence of Li^+. Data (means ± S.D.) are presented as percent of the respective control uptake in each case.

Biochemical Journal (2020) **477** 4149–4165
https://doi.org/10.1042/BCJ20200592

was dependent on the time period used for the preincubation with the inhibitor, with maximal inhibition evident at 30 min preincubation (Figure 2A). We carried out this experiment with and without Li^+ during the preincubation and during the uptake assay to determine if Li^+ alters the interaction of the transporter with the inhibitor. We found a small, but significant increase in the inhibitory potency when the preincubation with the inhibitor was done in the presence of Li^+. These data showed that when the cells were washed following the preincubation with BI01383298, the inhibition persisted, indicating that the inhibitor stayed bound to the transporter following the initial preincubation. We then determined the inhibitory potency for the compound using these experimental conditions (i.e. preincubation with the inhibitor for 30 min, then uptake assay in the absence of the inhibitor). The IC_{50} values for the inhibition under these conditions were 197 ± 51 nM in the absence of Li^+; 82 ± 10 nM in the presence of Li^+ (Figure 2B). These values were ∼2-fold higher compared with the corresponding values when the inhibitor was present during preincubation as well as during the uptake assay (118 ± 22 nM in the absence of Li^+; 49 ± 3 nM in the presence of Li^+).

To investigate how long the inhibitory effect of BI01383298 preincubation lasts, we performed recovery experiments for citrate uptake by HepG2 cells. The cells were preincubated with 10 μM BI01383298 for 30 min in NaCl buffer (pH 7.5) or the regular culture medium for HepG2 cells. Subsequent to this preincubation, the cells were washed to remove any free, unbound, inhibitor and then Na^+-dependent citrate uptake was measured for 30 min either immediately (zero time) or after maintaining the cells in the NaCl buffer or the culture medium for the indicated time periods. In the NaCl buffer, the preincubation caused almost complete inhibition of citrate uptake and the inhibition failed to recover even after 1 h (Figure 3A). In the culture medium, the inhibition did recover partially after 24 h (Figure 3B). The activity after this 24 h period was 18% of control uptake; the corresponding value at zero time was <5% of control uptake. Subsequent experiments showed that the significant recovery in transport activity observed when the cells, which were pre-exposed to the inhibitor, were allowed to remain in the culture medium for 24 h in the absence of the inhibitor was actually due to proliferation of new cells which never came in contact with the inhibitor.

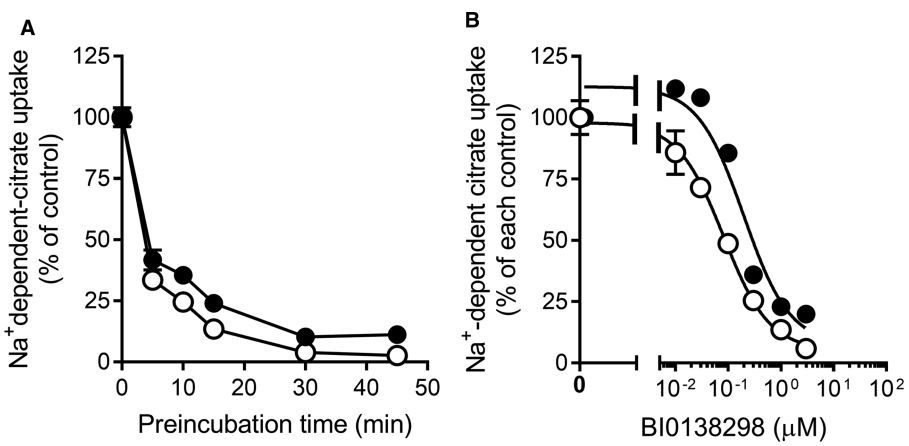

Figure 2. Effect of preincubation time with BI01383298 on NaCT-mediated citrate uptake in HepG2 cells.

(**A**) HepG2 cells were preincubated in NaCl buffer, pH 7.5, either without (●) or with 10 mM LiCl buffer (○) in the absence or presence of 10 μM BI01383298 for the indicated time periods. Cells were then washed twice to remove the inhibitor and then used for uptake measurement. Uptake of [^{14}C]-citrate was measured for 30 min with the respective preincubation buffer, but in the absence of BI01383298 (the inhibitor was present only during preincubation but absent during uptake). (**B**) HepG2 cells were preincubated in NaCl buffer, pH 7.5, either without (●) or with 10 mM LiCl buffer (○) with increasing concentrations of BI01383298 for 30 min. Cells were then washed twice to remove the inhibitor and then used for uptake measurement. Uptake of [^{14}C]-citrate was measured for 30 min with the preincubation buffer but in the absence of BI01383298 (the inhibitor was present at different concentrations only during preincubation but absent during uptake). The uptake values were higher when measured in the presence of Li^+ than in the absence of Li^+ as expected of human NaCT. The concentration of citrate was 7.0 μM for the uptake assay in the absence of Li^+, and 3.5 μM for the uptake assay in the presence of Li^+. Data (means ± S.D.) are presented as percent of the respective control uptake in each case.

Biochemical Journal (2020) **477** 4149–4165
https://doi.org/10.1042/BCJ20200592

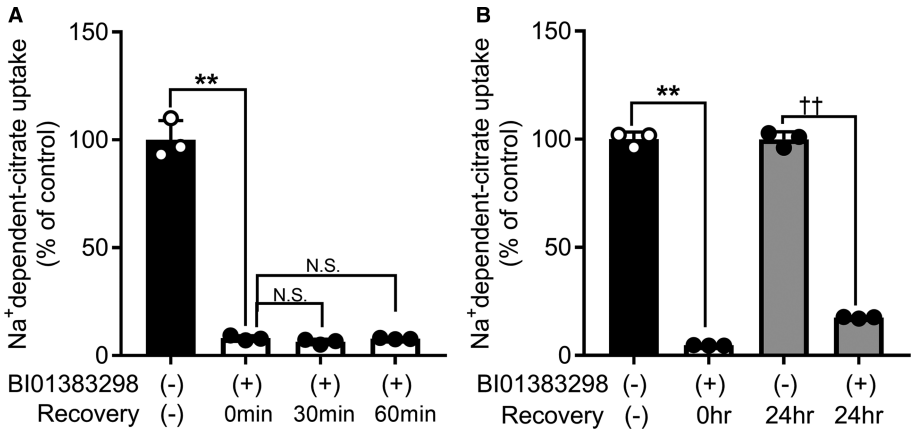

Figure 3. Irreversible nature of the inhibition by BI01383298 on NaCT-mediated citrate uptake in HepG2 cells.

HepG2 cells were preincubated in NaCl buffer, pH 7.5 (**A**) or culture medium (**B**) with or without 10 μM BI01383298 for 30 min. Cells were then washed twice with NaCl buffer, pH 7.5 and then incubated with either NaCl buffer, pH 7.5 for 0, 30 min or 60 min (**A**) or culture medium (**B**) for 0 or 24 h prior to use in uptake measurements. Uptake of [^{14}C]-citrate was measured for 30 min in the NaCl buffer (pH 7.5) with 10 mM LiCl buffer. The concentration of citrate was 3.5 μM during the uptake assay. Each column represents the mean ± S.D. $^{**}P < 0.01$ (ANOVA, Dunnett's post-hoc test or two-tailed, unpaired Student's *t*-test); N.S., not significant; $^{††}P < 0.01$ (Two-tailed, unpaired Student's *t*-test).

Specificity of BI0138298 for inhibition of citrate uptake

To examine whether the preincubation with BI01383298 affects only citrate uptake, we preincubated HepG2 cells with 10 μM BI01383298 for 30 min, and then washed the cells to remove free, unbound, inhibitor. The cells were then used for measurement of uptake with various compounds that are known to be transportable substrates for specific transporters other than NaCT/SLC13A5. We found that BI01383298 inhibited only citrate uptake. The substrates whose uptake was not affected by the inhibitor were nicotinate (substrate for SLC5A8 in the presence of Na^+), arginine (substrate for SLC6A14 in the presence of Na^+ and for SLC7A1 in the absence of Na^+), glutamine and tryptophan (substrates for SLC7A5 in the absence of Na^+), and lactate (substrate for MCTs in the absence of Na^+ but in the presence of an acidic pH) (Table 1).

Table 1 Effect of BI01383298 on the uptake function of different transporters in HepG2 cells monitored with appropriate substrates and experimental conditions

Substrate	Control	BI01383298	% Control
Citrate (7 μM)	483 ± 13	88.2 ± 5.6	18 ± 1**
Nicotinate (8 μM)	124 ± 3	123 ± 4	100 ± 3
Arginine (5 μM)	928 ± 31	935 ± 51	101 ± 5
Glutamine (5 μM)	319 ± 25	306 ± 3	92 ± 1
Tryptophan (5 μM)	80 ± 2	76 ± 3	95 ± 3
Lactate (3 μM)	141 ± 14	137 ± 7	97 ± 5

HepG2 cells were preincubated in NaCl buffer with or without 10 μM BI01383298 for 30 min. After washing the cells, uptakes of [^{14}C]-citrate, [^{14}C]-nicotinate, [^{3}H]-arginine, [^{3}H]-glutamine, [^{3}H]-tryptophan, and [^{14}C]-lactate were measured for a given time (which varied for different transporters) in NaCl buffer pH 7.5 (citrate, nicotinate, arginine), NMDG buffer pH 7.5 (glutamine, tryptophan) or NMDG pH 6 (lactate). The units for the uptake activity were pmol/mg of protein/30 min for citrate, pmol/mg of protein/15 min for nicotinate, arginine, glutamine, and tryptophan, and pmol/mg of protein/3 min for lactate. Data represent means ± S.D. $^{**}P < 0.01$ compared with the corresponding control uptake.

Biochemical Journal (2020) 477 4149–4165
https://doi.org/10.1042/BCJ20200592

Species-specific inhibition of human NaCT/SLC13A5 by BI01383298

We confirmed the inhibition of human NaCT/SLC13A5 by 10 μM BI01383298 using HEK293FT cells that were made to express human SLC13A5 ectopically (Figure 4A). Here the cells were preincubated with the inhibitor for 30 min and then citrate uptake was measured without the inhibitor in the uptake buffer. Under the same experimental conditions, ectopically expressed mouse NaCT/Slc13a5 was not inhibited by 10 μM BI01383298 (Figure 4B). We then examined the dose-response relationship for the inhibition of the cloned human NaCT/SLC13A5 with 30 min preincubation with the inhibitor and then uptake measurement in the absence of the inhibitor in the uptake medium. The IC_{50} value for the inhibition was calculated to be 171 ±

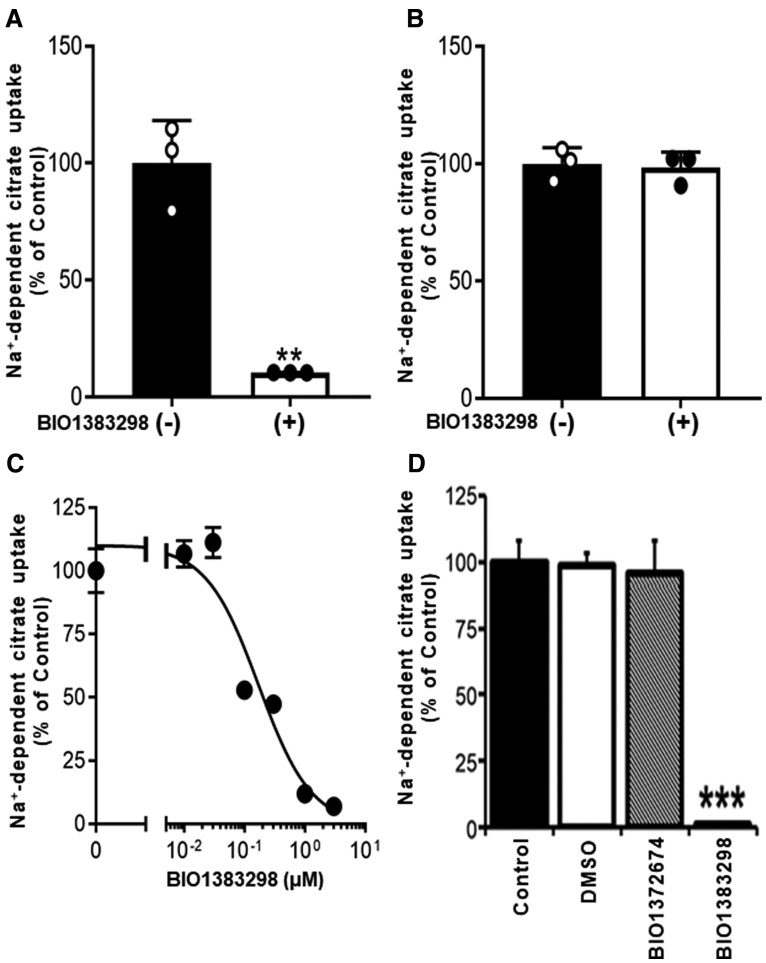

Figure 4. Differential effect of BI01383298 on human NaCT versus mouse NaCT.

The effects of BI01383298 on citrate uptake in HEK293FT cells with transient ectopic expression of human NaCT (SLC13A5) (**A**,**C**,**D**) or mouse NaCT (Slc13a5) (**B**) were examined. After transfection with the respective expression plasmids, cells were preincubated in NaCl buffer, pH 7.5 with or without 10 μM BI01383298 for 30 min. Cells were then washed twice prior to uptake measurements. Uptake of [^{14}C]-citrate (2 μM) was measured for 30 min in the NaCl buffer, pH 7.5. Each column represents the mean ± S.D. $^{**}P < 0.01$ compared with the uptake in control cells without preincubation with BI01383298 (ANOVA, Dunnett's post-hoc test). (**C**) Dose-response relationship for inhibition of uptake via human SLC13A5 by BI01383298. HEK293FT cells with transient ectopic expression of human NaCT (SLC13A5) were exposed to varying concentrations of the inhibitor only during the 30 min preincubation. Cells were then washed twice to remove the inhibitor and then uptake of [^{14}C]-citrate (2 μM) was measured for 30 min in the NaCl buffer, pH 7.5. (**D**) Evidence for the lack of inhibitory effect for vehicle control (0.1% dimethylsulfoxide) or the inactive chemical analogue BI01372674 on citrate transport via the ectopically expressed human NaCT in HEK293 cells. $^{***}P < 0.001$ compared with control uptake.

51 nM (Figure 4C). This value was identical with the corresponding value for the inhibition of the constitutively expressed NaCT/SLC13A5 in HepG2 cells (197 ± 51 nM; Figure 2B). The vehicle control (0.1% dimethylsulfoxide) or the inactive chemical analogue BI01372674 (10 μM) had no effect on human NaCT/SLC13A5 when the active compound BI01383294 at 10 μM caused complete inhibition of the transporter activity under identical conditions (Figure 4D).

The apparent irreversibility of the inhibition raised the question: is the inhibition competitive or non-competitive? To address this question, HepG2 cells were preincubated with or without 0.3 μM BI01383298 for 30 min and then washed to remove free, unbound, inhibitor. There was no citrate in the medium during the preincubation. The cells were then used for measurement of citrate uptake in a NaCl buffer over a citrate concentration range of 0.5–30 mM. The data are shown in Figure 5. After subtracting the diffusional component, which was calculated theoretically as described in the Methods section, the carrier-mediated uptake was analyzed by Eadie–Hofstee plot to determine the Michaelis constant (K_t) and maximal velocity (V_{max}). In the absence of the inhibitor, the values for K_t and V_{max} were 630 ± 135 μM and 94 ± 6 nmol/mg of protein/30 min. The corresponding values in the presence of the inhibitor were 445 ± 180 μM and 22 ± 3 nmol/mg of protein/30 min. These data show that the inhibition of NaCT/SLC13A5 by BI01383298 is non-competitive.

We then compared the inhibitory effect of BI01383298 with that of PF06761281, a recently reported high-affinity inhibitor of NaCT. The was first done with HepG2 cells for the constitutively expressed SLC13A5. The presence of PF06761281 (100 μM) or BI01383298 (10 μM) only during uptake measurement inhibited Na^+-dependent citrate uptake (Figure 6A). Both compounds inhibited NaCT transport activity. When the cells were preincubated (30 min), washed, and then used for citrate uptake, the magnitude of inhibition decreased for PF06761281 but increased for BI01383298. This shows that the inhibition of SLC13A5 by PF06761281 is at least partly reversible whereas the inhibition by BI01383298 is not. The magnitude of inhibition was greater with BI01383298 than with PF06761281, showing that the inhibitory potency for BI01383298 is at least 10 times greater than that for PF06761281. Almost exactly similar results were obtained for human SLC13A5 expressed ectopically in HEK293FT cells (Figure 6B). We then examined if the inhibition by PF06761281 is selective for human SLC13A5 as was the case for BI01383298. For this, we used the cloned mouse NaCT/Slc13a5 expressed ectopically in HEK293FT cells. In contrast with BI01383298, PF06761281 was able to inhibit the activity of mouse NaCT/Slc13a5 (Figure 6C). In fact, the inhibitory potency of PF06761281 for mouse NaCT/Slc13a5 was greater than for human NaCT/SLC13A5.

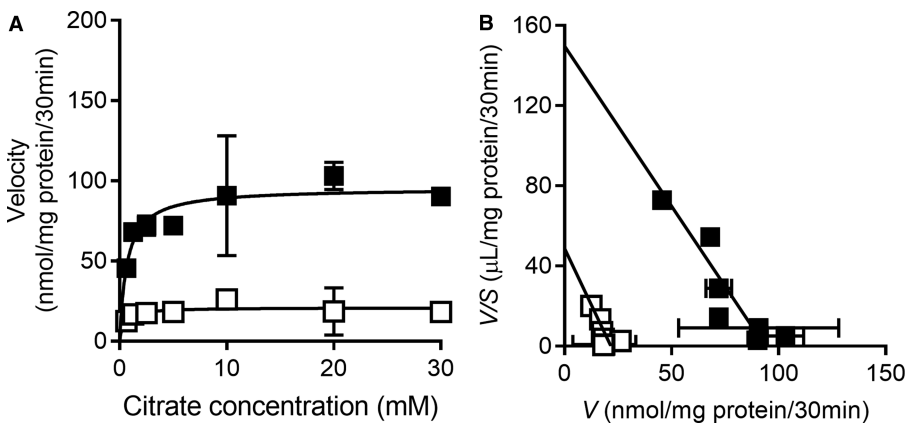

Figure 5. Kinetics of BI01383298-mediated inhibition on human NaCT (SLC13A5) in HEK293FT cells.

Cells with transient ectopic expression of human SLC13A5 were preincubated with NaCl buffer, pH 7.5 in the absence or presence of 0.3 μM BI01383298 for 30 min. After washing the cells twice, uptake of [^{14}C]-citrate tracer was measured for 30 min in NaCl buffer, pH 7.5 in the presence of unlabeled citrate (0.5 mM–30 mM). (**A**) Michaelis–Menten plot for the saturable component of the uptake in absence (■) or presence (□) of BI01383298; the saturable component was determined by subtracting the diffusional component from total uptake as described in the Methods section. (**B**) Eadie–Hofstee plot for the data in (**A**): *V* represents uptake velocity (nmol/mg protein/30 min) and *S* represents concentration of citrate (mM). Data are presented as mean ± S.D.

Biochemical Journal (2020) **477** 4149–4165
https://doi.org/10.1042/BCJ20200592

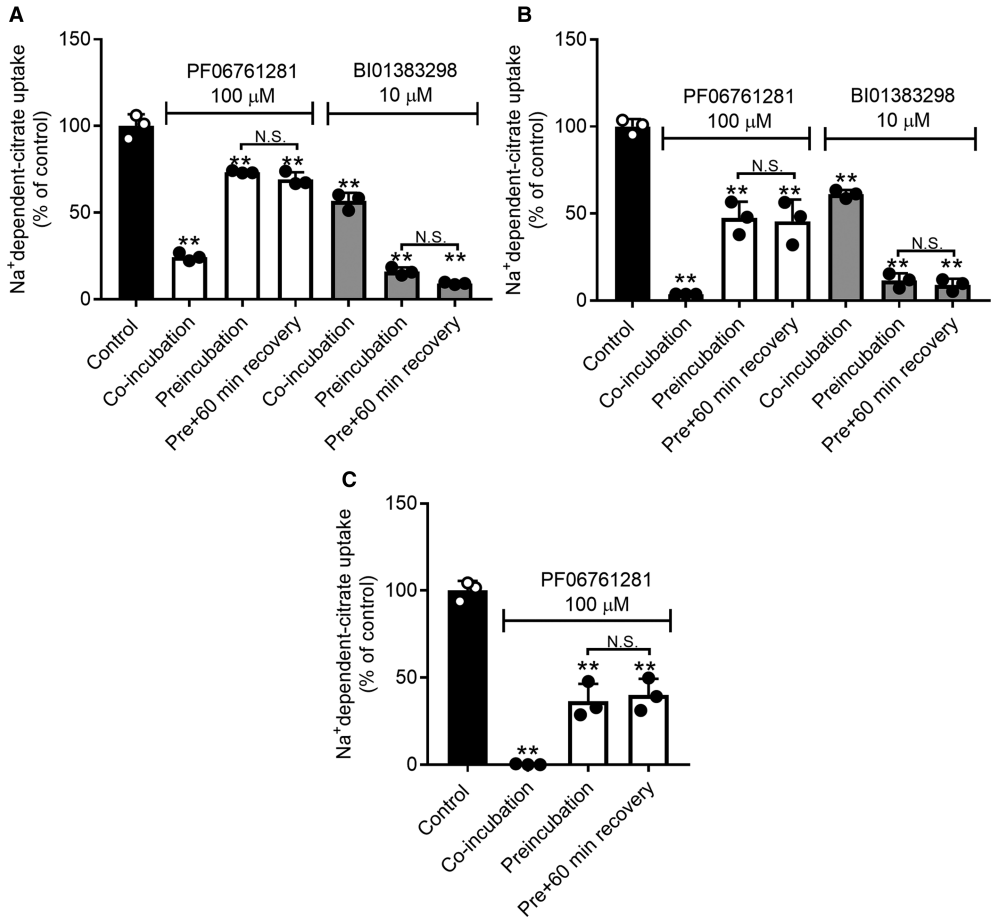

Figure 6. Comparison of the inhibitory effects of PF06761281 and BI01383298 on NaCT-mediated citrate uptake.
(**A**) HepG2 cells; (**B**) HEK293FT cells with ectopic expression of human NaCT (SLC13A5); (**C**) HEK293FT cells with transient ectopic expression of mouse NaCT (Slc13a5). Cells were preincubated in NaCl buffer, pH 7.5 without or with 100 μM PF0676181 or 10 μM BI01383298 for 30 min. Cells were then washed twice to remove the inhibitor and incubated with NaCl buffer, pH 7.5 for 0 (Preincubation, but no recovery) or 60 min (Preincubation with 60 min recovery). Following this, uptake of [^{14}C]-citrate (2 μM) was measured for 30 min in NaCl buffer, pH 7.5 in the absence (control, Preincubation and Preincubation plus 60 min recovery) or presence (co-incubation) of 100 μM PF0676181 or 10 μM BI01383298. Each column represents the mean ± S.D. ** $P < 0.01$ compared with uptake in cells without preincubation with either of the inhibitors (ANOVA, Tukey's post-hoc test). N.S., not significant.

Effect of BI01383298 on HepG2 cell proliferation

SLC13A5 provides cells with citrate to participate in several anabolic pathways and in energy production. Therefore, we examined the effect of BI01383298 as the potent inhibitor of SLC13A5 on HepG2 cell proliferation. These studies were done in the regular culture medium, but with 0.5 mM citrate as a supplement. Using the colony formation assay, we found robust inhibition of cell proliferation by BI01383298 (Figure 7).

Homology modeling of human NaCT and mouse NaCT

The human NaCT and the mouse NaCT homology models were based on the 2.78 Å resolution X-ray crystal structure of the humanized variant of the bacterial homologue VcINDY (PBD: 5ULD) [23]. VcINDY is a homodimer, where each monomer is composed of 11 transmembrane α-helices, and two helix-turn-helix hairpins (HP_{in} and HP_{out}). Even though the parent *Vibrio* transporter was referred to as INDY, its substrate selectivity is different from that of the *Drosophila* and mammalian INDY (NaCT/SLC13A5). The parent *Vibrio* transporter accepts the dicarboxylate succinate as the substrate; in contrast, NaCT/mINDY prefers the

Biochemical Journal (2020) **477** 4149–4165
https://doi.org/10.1042/BCJ20200592

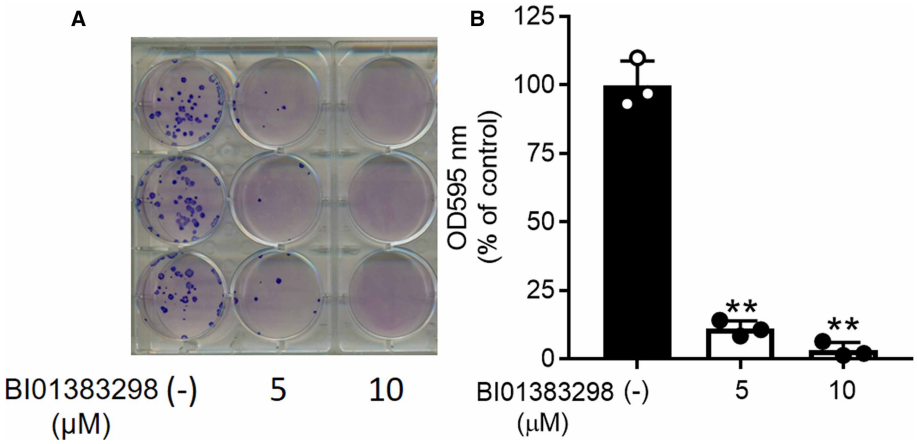

Figure 7. Inhibitory effect of BI01383298 on proliferation of HepG2 cells.

Cell proliferation was assessed using the colony formation assay with 0, 5, and 10 μM of the inhibitor. (**A**) Documentation of colonies. (**B**) Quantification of Geimsa stain. ** $P < 0.01$ compared with control (i.e. absence of the inhibitor).

tricarboxylate citrate over succinate as the substrate. Therefore, to make the structure of the parent *Vibrio* transporter relevant to mINDY, a humanized variant was generated; the humanized variant contains the same overall sequence as the *Vibrio* succinate transporter, but eight 'humanized' mutations were included at the citrate-binding site to favor selectivity for citrate instead of succinate. Each of the two Na^+ and the citrate binding sites are formed by residues of the two hairpin structures (HP_{in} and HP_{out}), particularly the Serine-Asparagine-Threonine (SNT) motifs. VcINDY and NaCT are part of divalent anion–sodium symporter (DASS) family, where the SNT motif is highly conserved [28].

Human NaCT (Figure 8A) and mouse NaCT (Figure 8B) share high primary sequence similarity to the humanized VcINDY (75% similarity, 29% identity). Because of this similarity, each was modeled as a homodimer similar to VcINDY. The models have 11 transmembrane spans, a set of two hairpin (HP_{in} and HP_{out}) and adjacent discontinuous helices in each monomer similar to VcINDY. In each set, the inter-helical loops of the hairpins (HP_{in} and HP_{out}), and the intra-helical loops of the adjacent discontinuous TM5 and TM10 helices, respectively, form a cleft that opens toward the cytoplasm. Both human and mouse transporters show long loops in the cytoplasm, similar to previously published human NaCT models [16,29–33].

Binding sites for citrate, BI01383298, and PF-06761281

Citrate (substrate) and BI01383298 (inhibitor) were docked using homology models of human NaCT and mouse NaCT showing a proposed binding site of these molecules. The computed binding affinities for citrate for interaction with human NaCT and mouse NaCT are −2.4 kcal/mol and −4.2 kcal/mol, respectively. This suggests that citrate has at least 10-fold higher affinity for mouse NaCT than for human NaCT (a difference of 1.4 kcal/mol in binding energy equals a 10-fold difference in binding affinity). This has been documented experimentally [9,10]. Residues Ser140, Asn141, and Thr142 (HP_{in}) from the first SNT, Asn465 (HP_{out}) from the second SNT, Thr227 and Gly228 (TM5b), and Ser499 (TM10a) interact with citrate in highest affinity docking poses of human NaCT (Figure 9A). These residues are identical with residues in VcINDY involved in citrate binding. Mouse NaCT shows largely similar binding residues for citrate except for one less binding residue near the first Na^+-binding site (Na1) but an additional binding residue (Thr512), which is not apparent in human NaCT (Figure 9B). The inhibitor BI01383298 docks in the same binding pocket as the citrate (Figure 9C,D). The computed binding affinities for BI01383298 for interaction with human NaCT and mouse NaCT are −6.8 kcal/mol and −5.8 kcal/mol, respectively. This suggests that the inhibitor has higher affinity for human NaCT than for mouse NaCT, again supported by direct experimental evidence in the present study. BI01383298 interacts with Thr227 and Gly228 (TM5b), and Ser464, Asn465 and Val466 (HP_{out}) residues in human NaCT (Figure 9C). In contrast, only Thr142 and Ser468 participate in mouse NaCT for interaction with the inhibitor (Figure 9D). The lack of multiple binding residues for the inhibitor in mouse NaCT is

Biochemical Journal (2020) **477** 4149–4165
https://doi.org/10.1042/BCJ20200592

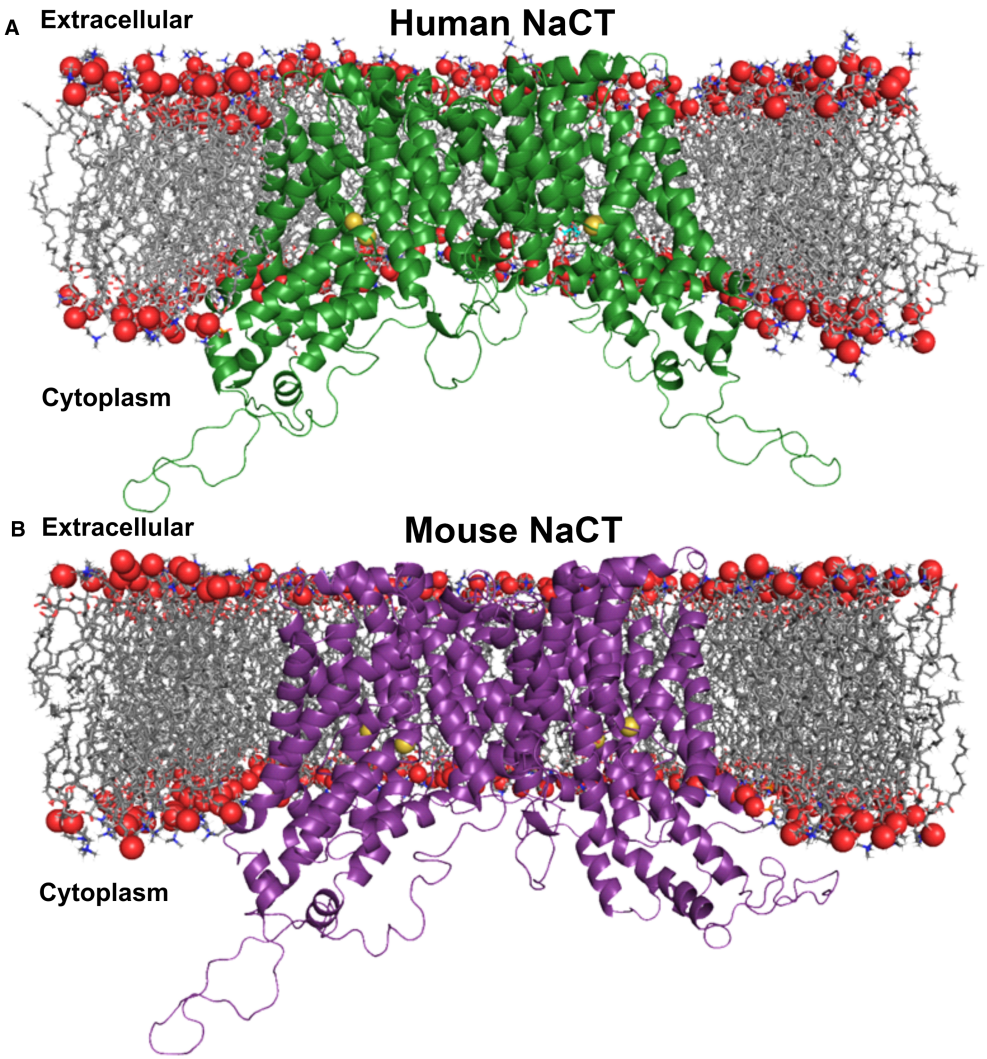

Figure 8. Homology modeling of human and mouse NaCT.

(**A**) Ribbon representation of the human NaCT homodimer in the inward-facing conformation. The homology model was embedded in a DOPC phospholipid bilayer for molecular dynamics simulation. (**B**) Ribbon diagram of the mouse NaCT homodimer in the inward-facing conformation embedded in a DOPC phospholipid bilayer. Red spheres are phosphates and grey sticks are the diacylglycerol backbone of phosphatidylcholine, the most abundant lipid in animal cell membranes. Each monomer forms an internal cavity with a Na^+ (yellow spheres) and citrate (cyan sticks), adjacently bound to each pocket at the cytosolic basin of the protomer. Citrate ions are exposed to the cytosolic space whereas the Na^+ ions are buried.

probably the reason for the little or no inhibition of mouse NaCT by this compound in contrast with human NaCT, which is inhibited at nanomolar concentrations of the same compound.

The other inhibitor, PF-06761281, also docks to the same binding pocket as citrate. The hydroxysuccinic acid moiety of the compound interacts with Asn143 (HP_{in}), Thr229 and Gly230 (TM5b), and Asn465(HP_{out}). The methoxy group in the 2-methoxy-5-methyl-3-pyridinyl ring of the compound forms van der Waals interactions with the backbone amide of Gly228 in human NaCT or Gly231 in mouse NaCT. The computed binding affinities for this inhibitor for interaction with human NaCT and mouse NaCT are −6.6 kcal/mol and −7.2 kcal/mol, respectively. This suggests higher affinity of the compound for mouse NaCT than for human NaCT, which is supported by the more potent inhibitory potency of the compound for mouse NaCT than for human NaCT.

Biochemical Journal (2020) **477** 4149–4165
https://doi.org/10.1042/BCJ20200592

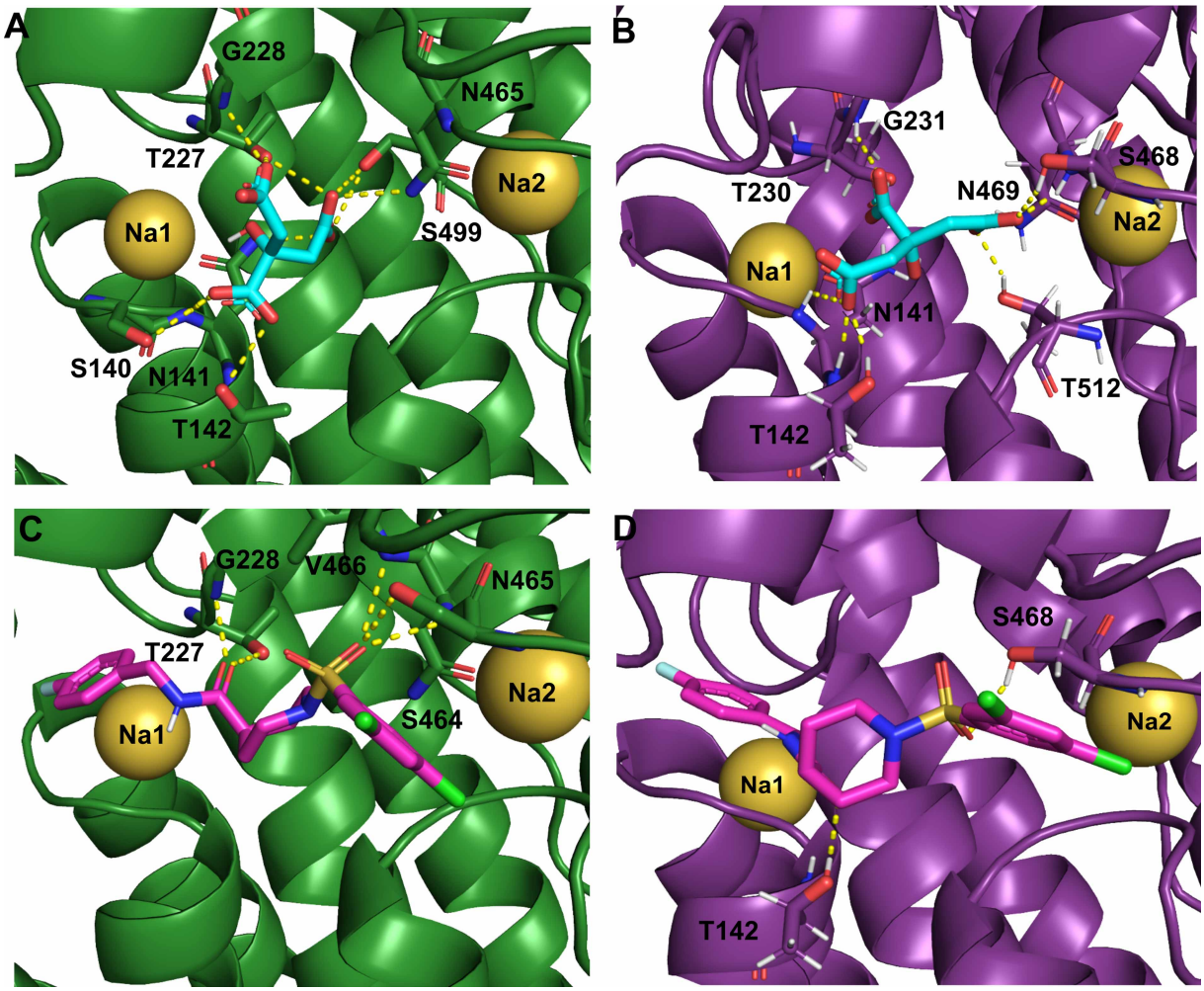

Figure 9. Closeup view of the proposed the binding sites for citrate and BI01383298 in human NaCT and mouse NaCT.
Citrate ion (cyan) binding to human NaCT (A) and mouse NaCT (B). BI01383298 (magenta) binding to human NaCT (C) and mouse NaCT (D). Na^+ ions are shown as yellow spheres.

Discussion

This is the first report on the identification of a high-affinity irreversible inhibitor of human NaCT. The high-affinity nature of this inhibitor (BI01383298) has been documented in the datasheet available from the commercial suppliers of this compound (e.g. MedKoo Biosciences, Millipore Sigma, TOCRIS). However, it was not known that it is an irreversible inhibitor. The studies described in the present report provide supporting evidence for the irreversible nature of the inhibition caused by this compound. We do not know whether the inhibitor covalently modifies the transporter at its binding site or the irreversible inhibition is simply caused by the high-affinity interaction with the transporter. The compound does contain Cl and F residues attached to benzene rings (Figure 10) which could potentially help in the covalent interaction of the compound with specific serine residues involved in the docking of the compound at the binding site. But covalent modification is not mandatory to elicit irreversible inhibition. If the binding of the inhibitor with the transporter protein is tight enough due to high affinity, irreversible inhibition could ensue. The experimental data from the current study nor the molecular modeling and docking approaches are able to differentiate between these two possibilities. Even though the inhibition is irreversible, the interaction of BI01383298 with human NaCT is not instantaneous but is a time-dependent process; the longer the time of incubation of the cells with the inhibitor, the greater is the magnitude of inhibition. It is probable that the binding of BI01383298 to the transporter induces

Biochemical Journal (2020) 477 4149–4165
https://doi.org/10.1042/BCJ20200592

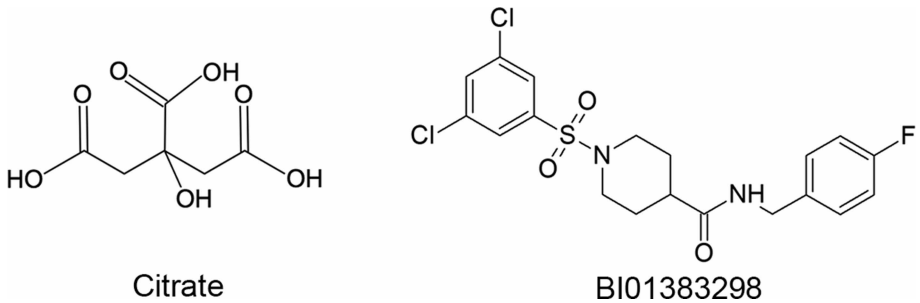

Figure 10. Chemical structures of the transportable substrate citrate and the irreversible inhibitor BI01383298.

conformational changes in the protein, thus altering the binding pocket for citrate and hence inhibiting the transport function. Additional studies would be needed to address these issues. It is also interesting that the transportable substrate citrate and the irreversible inhibitor BI01383298 bind almost to the same region in the transporter despite the fact that the chemical structures and 3D-structures of these two compounds are vastly different (Figure 10). The inhibition of citrate transport via human NaCT by BI01383298 is non-competitive despite the fact that both the substrate and the inhibitor interact with the same region of the transporter. The non-competitive nature of this inhibition is not surprising because the irreversible interaction of the inhibitor with the transporter essentially decreases the density of the unaffected transporter in the cell, thus causing the non-competitive inhibition. As the Michaelis constant is independent of the transporter density whereas the maximal velocity of transport activity is directly proportional to the transporter density, a decrease in the number of unaffected transporter molecules in the presence of the inhibitor is expected to decrease the maximal velocity of the transport activity without affecting the Michaelis constant. If BI01383298 were to be reversible inhibitor, it is very likely that the kinetics of inhibition would have turned out to be competitive in nature.

The species specificity is another important and interesting aspect of this inhibitor. BI01383298 inhibits human NaCT with an IC_{50} of ∼100 nM. But the mouse NaCT is not inhibited by this compound even at 10 μM, a concentration 100 times higher than the IC_{50} for human NaCT. This highlights the functional differences between human NaCT and mouse NaCT, which have been known for a long time but failed to receive adequate attention or recognition. We have documented that human NaCT has at least 30-fold lower affinity for citrate than mouse NaCT even when the kinetic experiments are done under identical conditions [9,10]. This difference seems to hold between any primate NaCT (human, monkey, chimpanzee) and rodent NaCT (mouse, rat) [11]. Another remarkable difference between human (and other primates) NaCT and mouse (and rat) NaCT is the differential effect of Li^+. In the presence of Na^+, primate NaCT is markedly activated by Li^+ whereas rodent NaCT is inhibited by Li^+ [11]. Neither transporter is functional in the total absence of Na^+, but Li^+ stimulates human NaCT and inhibits mouse NaCT in the presence of Na^+. All mammalian NaCTs (human as well as mouse) transport citrate in its trivalent anionic form coupled to the co-transport of 4 Na^+, thus making the transport process electrogenic. The stimulatory effect of Li^+ on human NaCT could be explained if one or more, but not all, of the Na^+-binding sites accept Li^+ with a much higher affinity than the affinity with which they interact with Na^+. We are however unable to provide a reasonable explanation for the inhibition of mouse NaCT by Li^+. The differential effect of BI01383298 is an important addition to the functional differences between human and mouse NaCTs [33]. These differences assume significant biological importance given the fact that loss-of-function mutations in NaCT cause a severe form of early infantile epileptic encephalopathy in humans, a disease identified as EIEE-25 (Early Infantile Epileptic Encephalopathy-25). In contrast, deletion of the transporter in mice is associated with no detrimental phenotype; it actually leads to a beneficial phenotype, providing protection against diet-induced obesity and diabetes [34]. This raises valid questions as to the suitability of mouse or rat as an experimental model to investigate and understand the biological aspects of NaCT in humans.

Deletion of NaCT leads to beneficial effects in the liver but detrimental effects in the brain. The *Slc13a5*-null mice which lack NaCT are protected from diet-induced obesity, diabetes, and metabolic syndrome [13]. This is congruent with the known biological functions of citrate in the liver where citrate levels are regulated by NaCT. Our recent studies have shown that metformin, the most widely used anti-diabetic drug, suppresses the

expression of NaCT in HepG2 cells, thus another mode of action of the drug to explain its therapeutic efficacy in diabetes [35]. In the brain, NaCT seems to play a critical role in the maintenance of normal neuronal function; as such, disruption of its function results in deleterious consequences as seen in humans with loss-of-function mutations in the transporter. Therefore, pharmacologic inhibitors of NaCT which will work peripherally without getting access to the brain might have therapeutic potential as drugs for diet-induced obesity, diabetes, and metabolic syndrome. Another area where NaCT-specific inhibitors would have therapeutic potential is the liver cancer. Recent studies have shown that NaCT is up-regulated in hepatocellular carcinoma and that silencing of the transporter decreases the growth and proliferation of liver cancer cells *in vitro* and *in vivo* [36]. In the present study, we have demonstrated that BI01383298, the inhibitor selective for human NaCT, does block the proliferation of the human liver cell line HepG2, which expresses NaCT constitutively. These data support the rationale that NaCT-selective inhibitors might have potential as therapeutic agents for the treatment of liver cancer.

Given the background that blockade of NaCT function could be beneficial in various diseases, in most cases related to the liver, the identification of a high-affinity irreversible inhibitor for NaCT in the present study is of clinical and therapeutic significance. Nothing is known however on whether or not BI01383298 has any effect on diet-induced obesity, diabetes, metabolic syndrome or hepatocellular carcinoma *in vitro* or *in vivo*. There is also no information on the pharmacokinetics and pharmacodynamics of this compound *in vivo*. Such studies in experimental models using simple laboratory animals such as the mouse are not feasible for the most part because of the species-specificity of this compound as the selective inhibitor of human NaCT.

The molecular basis of species specificity of BI01383298 remains poorly understood in spite of the effort in the present study using molecular modeling and docking experiments. The primary reason for this is the inadequacy of the 3D-model of the human variant of VcINDY to understand the 3D-structure of human NaCT. We use the human variant of VcINDY as the structural model for human NaCT because it is the best substitute available at present for human NaCT. The inadequacy of this approach is readily obvious however, considering the fact that VcINDY bears only 29% identity with human NaCT in amino acid sequence. Even though specific amino acid substitutions were introduced in VcINDY to 'humanize' it at least in the substrate-binding domain, it is not the same as having the structure of human NaCT itself. We also do not know how the rest of the amino acid sequences in VcINDY influences the substrate-binding pocket in spite of the selective amino acid substitutions. The deficiency of this approach is even more evident in the case of the Na^+-binding sites. Only two Na^+-binding sites are predicted in the humanized VcINDY as shown in Figure 9, but the number of Na^+-binding sites in human NaCT is expected to be at least 4 based on the electrogenic nature of the NaCT-mediated transport of the trivalent anion $citrate^{3-}$. Despite these issues, the molecular modeling does pinpoint structural differences between human NaCT and mouse NaCT and also provide at least some molecular insight into the marked differences in citrate affinity and BI01383298 affinity for human NaCT versus mouse NaCT. A more clear-cut understanding of this phenomenon has to wait until the 3D-structure of human NaCT is elucidated.

Competing Interests

The authors declare no conflict of interest. Pfizer Inc. supplied PF06761281 to us, but they had no role in the design of the study, in the collection, analyses, or interpretation of data, or in the decision to publish the results.

Funding

This work was supported by the Welch Endowed Chair in Biochemistry, Grant No. BI-0028, at Texas Tech University Health Sciences Center.

Open Access

Open access for this article was enabled by the participation of the Texas Tech University Health Sciences Center in an all-inclusive *Read & Publish* pilot with Portland Press and the Biochemical Society under a transformative agreement with EBSCO.

Author Contribution

K.H. contributed the most in performing the uptake experiments; J.J.K. and S.S. also made significant contributions in completing the uptake experiments; V.J.M. and R.B.S. did the molecular modeling and docking studies; I.L.U. edited the section related to molecular modeling and docking experiments; V.G. designed the experiments and interpreted the data; K.H., V.J.M., and V.G. wrote the manuscript.

Biochemical Journal (2020) **477** 4149–4165
https://doi.org/10.1042/BCJ20200592

Acknowledgements

The authors acknowledge the High Performance Computing Center (HPCC; URL: http://cmsdev.ttu.edu/hpcc) at Texas Tech University at Lubbock for providing High Performance computing services that have contributed to the data reported in this paper.

Abbreviations

DOPC, 1,2-dioleoyl-sn-glycero-3-phosphocholine; FBS, fetal bovine serum; HP, helix-turn-helix hairpin; INDY, I'm Not Dead Yet; mINDY, mammalian INDY; NaCT, Na^+-coupled citrate transporter; NMDG, *N*-methyl-D-glucamine; SLC13A5, solute carrier gene family 13A member 5; TM, transmembrane domain; VcINDY, *Vibrio cholerae* INDY.

References

1 Wagh, A. and Stone, N.J. (2004) Treatment of metabolic syndrome. *Expert Opin. Cardiovasc. Ther.* **2**, 213–228 https://doi.org/10.1586/14779072.2.2.213
2 Grundy, S.M. (2008) Metabolic syndrome pandemic. *Arterioscler. Thromb. Vasc. Biol.* **28**, 629–636 https://doi.org/10.1161/ATVBAHA.107.151092
3 Perez, E.A., Olivares, V.M., Martinez-Espinosa, R.M., Molina Vila, M.D. and Garcia-Galbis, M.R. (2018) New insights about how to make an intervention in children and adolescents with metabolic syndrome: Diet, exercise vs. changes in body composition. A systematic review of RCT. *Nutrients* **10**, 878 https://doi.org/10.3390/nu10070878
4 Willmes, D.M., Kurzbach, A., Henke, C., Schumann, T., Zahn, G., Heifetz, A. et al. (2018) The longevity gene INDY (I'm Not Dead Yet) in metabolic control: potential as pharmacologic target. *Pharmacol. Ther.* **185**, 1–11 https://doi.org/10.1016/j.pharmthera.2017.10.003
5 Rogina, B. (2017) INDY: a new link to metabolic regulation in animals and humans. *Front. Genet.* **8**, 66 https://doi.org/10.3389/fgene.2017.00066
6 Williams, N.C. and O'Neill, A.J. (2018) A role for the Krebs cycle intermediate citrate in metabolic reprogramming in innate immunity and inflammation. *Front. Immunol.* **9**, 141 https://doi.org/10.3389/fimmu.2018.00141
7 Myceilska, M.E., Patel, A., Rizaner, N., Mazurek, M.P., Keun, H., Patel, A. et al. (2009) Citrate transport and metabolism in mammalian cells: prostate epithelial cells and prostate cancer. *Bioessays* **31**, 10–20 https://doi.org/10.1002/bies.080137
8 Inoue, K., Zhuang, L., Maddox, D.M., Smith, S.B. and Ganapathy, V. (2002) Structure, function, and expression pattern of a novel sodium-coupled citrate transporter (NaCT) cloned from mammalian brain. *J. Biol. Chem.* **277**, 39469–39476 https://doi.org/10.1074/jbc.M207072200
9 Inoue, K., Zhuang, L. and Ganapathy, V. (2002) Human Na^+-coupled citrate transporter: primary structure, genomic organization, and transport function. *Biochem. Biophys. Res. Commun.* **299**, 465–471 https://doi.org/10.1016/S0006-291X(02)02669-4
10 Inoue, K., Fei, Y.J., Zhuang, L., Gopal, E., Miyauchi, S. and Ganapathy, V. (2004) Functional features and genomic organization of mouse NaCT, a sodium-coupled transporter for tricarboxylic acid intermediates. *Biochem. J.* **378**, 949–957 https://doi.org/10.1042/bj20031261
11 Gopal, E., Babu, E., Ramachandran, S., Bhutia, Y.D., Prasad, P.D. and Ganapathy, V. (2015) Species-specific influence of lithium on the activity of SLC13A5 (NaCT): lithium-induced activation is specific for the transporter in primates. *J. Pharmacol. Exp. Ther.* **353**, 17–26 https://doi.org/10.1124/jpet.114.221523
12 Gopal, E., Miyauchi, S., Martin, P.M., Ananth, S., Srinivas, S.R., Smith, S.B. et al. (2007) Expression and functional features of NaCT, a sodium-coupled citrate transporter, in human and rat livers and cell lines. *Am. J. Physiol. Gastrointest. Liver Physiol.* **292**, G402–G408 https://doi.org/10.1152/ajpgi.00371.2006
13 Birkenfeld, A.L., Lee, H.Y., Guebre-Egziabher, F., Alves, T.C., Jurczak, M.J., Jornayvaz, F.R. et al. (2011) Deletion of the mammalian INDY homolog mimics aspects of dietary restriction and protects against adiposity and insulin resistance in mice. *Cell Metab.* **14**, 184–195 https://doi.org/10.1016/j.cmet.2011.06.009
14 Sun, J., Aluvila, S., Kotaria, R., Mayor, J.A., Walters, D.E. and Kaplan, R.S. (2010) Mitochondrial and plasma membrane citrate transporters: Discovery of selective inhibitors and application to structure/function analysis. *Mol. Cell. Pharmacol.* **2**, 101–110 PMID:20686672
15 Huard, K., Brown, J., Jones, J.C., Cabral, S., Futatsugi, K., Gorgoglione, M. et al. (2015) Discovery and characterization of novel inhibitors of the sodium-coupled citrate transporter (NaCT or SLC13A5). *Sci. Rep.* **5**, 17391 https://doi.org/10.1038/srep17391
16 Pajor, A.M., de Oliveira, C.A., Song, K., Huard, K., Shanmugasundaram, V. and Erion, D.M. (2016) Molecular basis for inhibition of the Na^+/citrate transporter NaCT (SLC13A5) by dicarboxylate inhibitors. *Mol. Pharmacol.* **90**, 755–765 https://doi.org/10.1124/mol.116.105049
17 Huard, K., Gosset, J.R., Montgomery, J.I., Gilbert, A.M., Hayward, M.M., Magee, T.V. et al. (2016) Optimization of a dicarboxylic series for in vivo inhibition of citrate transport by the solute carrier 13 (SLC13) family. *J. Med. Chem.* **59**, 1165–1175 https://doi.org/10.1021/acs.jmedchem.5b01752
18 Rives, M.L., Shaw, M., Zhu, B., Hinke, S.A. and Wickenden, A.D. (2016) State-dependent allosteric inhibition of the human SLC13A5 citrate transporter by hydroxysuccinic acids, PF-06649298 and PF-06761281. *Mol Pharmacol.* **90**, 766–774 https://doi.org/10.1124/mol.116.106575
19 Yamashita, A., Singh, S.K., Kawate, T., Jin, Y. and Gouaux, E. (2005) Crystal structure of a bacterial homologue of Na^+/Cl^- -dependent neurotransmitter transporters. *Nature* **437**, 215–223 https://doi.org/10.1038/nature03978
20 Inoue, K., Zhuang, L., Maddox, D.M., Smith, S.B. and Ganapathy, V. (2003) Human sodium-coupled citrate transporter, the orthologue of drosophila indy, as a novel target for lithium action. *Biochem. J.* **374**, 21–26 https://doi.org/10.1042/bj20030827
21 Pei, J., Kim, B.H. and Grishin, N.V. (2008) PROMALS3D: a tool for multiple protein sequence and structure alignments. *Nucleic Acids Res.* **36**, 2295–2300 https://doi.org/10.1093/nar/gkn072
22 Sali, A. and Blundell, T.L. (1990) Definition of general topological equivalence in protein structures. A procedure involving comparison of properties and relationships through simulated annealing and dynamic programming. *J. Mol. Biol.* **212**, 403–428 https://doi.org/10.1016/0022-2836(90)90134-8
23 Nie, R., Stark, S., Symersky, J., Kaplan, R.S. and Lu, M. (2017) Structure and function of the divalent anion/Na^+ symporter from vibrio cholerae and a humanized variant. *Nat. Commun.* **8**, 15009 https://doi.org/10.1038/ncomms15009
24 Jo, S., Kim, T., Iyer, V.G. and Im, W. (2008) CHARMM-GUI: a web-based graphical user interface for CHARMM. *J. Comput. Chem.* **29**, 1859–1865 https://doi.org/10.1002/jcc.20945

25 Phillips, J.C., Braun, R., Wang, W., Gumbart, J., Tajkhorshid, E., Villa, E. et al. (2005) Scalable molecular dynamics with NAMD. *J. Comput. Chem.* **26**, 1781–1802 https://doi.org/10.1002/jcc.20289
26 Pettersen, E.F., Goddard, T.D., Huang, C.C., Couch, G.S., Greenblatt, D.M., Meng, E.C. et al. (2004) UCSF chimera: a visualization system for exploratory research and analysis. *J. Comput. Chem.* **25**, 1605–1612 https://doi.org/10.1002/jcc.20084
27 Trott, O. and Olson, A.J. (2010) Autodock Vina: improving the speed and accuracy of docking with a new scoring function, efficient optimization, and multithreading. *J. Comput. Chem.* **31**, 455–461 https://doi.org/10.1002/jcc.21334
28 Wan, W.Y. and Milner-White, E.J. (1999) A recurring two-hydrogen-bond motif incorporating a serine or threonine residue is found both at alpha-helical N termini and in other situations. *J. Mol. Biol.* **286**, 1651–1662 https://doi.org/10.1006/jmbi.1999.2551
29 Hardies, K., de Kovel, C.G.F., Weckhuysen, S., Asselbergh, B., Geuens, T., Deconinck, T. et al. (2015) Recessive mutations in SLC13A5 result in a loss of citrate transport and cause neonatal epilepsy, developmental delay and teeth hypoplasia. *Brain* **138**, 3238–3250 https://doi.org/10.1093/brain/aww263
30 Klotz, J., Proter, B.E., Colas, C., Schlessinger, A. and Pajor, A.M. (2016) Mutations in the Na^+/citrate cotransporter NaCT (SLC13A5) in pediatric patients with epilepsy and developmental delay. *Mol. Med.* **22**, 310–321 https://doi.org/10.2119/molmed.2016.00077
31 Selch, S., Chafai, A., Sticht, H., Birkenfeld, A.L., Fromm, M.F. and Konig, J. (2018) Analysis of naturally occurring mutations in the human uptake transporter NaCT important for bone and brain development and energy metabolism. *Sci. Rep.* **8**, 11330 https://doi.org/10.1038/s41598-018-29547-8
32 Khamaysi, A., Aharon, S., Eini-Rider, H. and Ohana, E. (2020) A dynamic anchor domain in slc13 transporters controls metabolite transport. *J. Biol. Chem.* **295**, 8155–8163 https://doi.org/10.1074/jbc.RA119.010911
33 Jaramillo-Martinez, V., Urbatsch, I.L. and Ganapathy, V. (2020) Functional distinction between human and mouse sodium-coupled citrate transporters and its biologic significance: an attempt for structural basis using a homology modeling approach. *Chem. Rev.* https://doi.org/10.1021/acs.chemrev.0c00529
34 Bhutia, Y.D., Kopel, J.J., Lawrence, J.J., Neugebauer, V. and Ganapathy, V. (2017) Plasma membrane Na^+-coupled citrate transporter (SLC13A5) and neonatal epileptic encephalopathy. *Molecules* **22**, 378 https://doi.org/10.3390/molecules22030378
35 Kopel, J.J., Higuchi, K., Ristic, B., Sato, T., Ramachandran, S. and Ganapathy, V. (2020) The hepatic plasma membrane citrate transporter NaCT (SLC13A5) as a molecular target for metformin. *Sci. Rep.* **10**, 8536 https://doi.org/10.1038/s41598-020-65621-w
36 Li, Z., Li, D., Choi, E.Y., Lapidus, R., Zhang, L., Huang, S.M. et al. (2017) Silencing of solute carrier family 13 member 5 disrupts energy homeostasis and inhibits proliferation of human hepatocarcinoma cells. *J. Biol. Chem.* **292**, 13890–13901 https://doi.org/10.1074/jbc.M117.783860